

Ambient to high temperature fracture toughness and fatigue-crack propagation behavior in a Mo–12Si–8.5B (at.%) intermetallic

H. Choe^a, D. Chen^a, J.H. Schneibel^b, R.O. Ritchie^{a,*}

^aMaterials Sciences Division, Lawrence Berkeley National Laboratory, and Department of Materials Science and Engineering,
University of California, Berkeley, CA 94720, USA

^bMetals and Ceramics Division, Oak Ridge National Laboratory, Oak Ridge, TN 37831, USA

Received 1 October 2000; accepted 18 January 2001

Abstract

Boron-containing molybdenum silicides have been the focus of significant research of late due to their potentially superior low-temperature “pest” resistance and high-temperature oxidation resistance comparable to that of MoSi_2 -based silicides; however, like many ordered intermetallics, they are plagued by poor ductility and toughness properties. Of the various multiphase Mo–Si–B intermetallic systems available, alloys with compositions of Mo–12Si–8.5B (at.%), which contain Mo, Mo_3Si , and T2 phases, are anticipated to have higher toughesses because of the presence of the relatively ductile Mo phase. In this study, we examine the ambient to high (1300°C) temperature fracture toughness (R-curve) and fatigue-crack growth characteristics of Mo–12Si–8.5B, with the objective of discerning the salient mechanisms governing crack growth. It is found that this alloy displays a relatively high *intrinsic* (crack-initiation) toughness at 800 up to 1200°C ($\sim 10 \text{ MPa}\sqrt{\text{m}}$), but only limited *extrinsic* R-curve (crack-growth) toughness. Although the lack of extrinsic toughening mechanisms is not necessarily beneficial to quasi-static properties, it does imply in a brittle material that it should show only minimal susceptibility to premature failure by fatigue, as is indeed observed at temperatures from ambient to 1300°C . Of particular significance is that both the fracture toughness and the threshold stress intensity for fatigue are increased with increasing temperature over this range. This remarkable property is related to a variety of toughening mechanisms that become active at elevated temperatures, specifically involving crack trapping by the α -Mo phase and extensive microcracking primarily in the Mo_5SiB_2 phase. Published by Elsevier Science Ltd.

Keywords: A. Intermetallics miscellaneous; B. Fracture toughness

1. Introduction

The quest for structural materials that can operate at higher and higher temperatures remains a persistent challenge in materials science. The current best prospects in this regard are probably ceramic- and intermetallic-matrix composites although, since their cost is prohibitive for many applications, much recent work has focused on their monolithic counterparts. In the intermetallics field, perhaps the most progress has been made with alloys based on nickel and especially titanium aluminides. These alloys can exhibit significant room temperature ductility, at least compared to other intermetallics, but have the major disadvantage that

their operating temperatures would be limited to less than 1000°C , which is too low for many future applications [1]. One candidate material which could be used at significantly higher temperatures is molybdenum disilicide, due to its excellent oxidation resistance, high melting temperature, and relatively easy processibility. However, the structural use of molybdenum silicides is severely limited by their low ductility and poor fracture toughness at ambient temperatures.

In an attempt to enhance the ductility and fracture toughness of these alloys, one approach is through *in situ* ductile-phase toughening. The idea here is to process the silicide with excess Mo; then provided the crack intercepts the resulting primary α -Mo phase, catastrophic fracture can be hindered through the formation of unbroken ductile-particle ligaments in the crack wake. The resulting crack bridging and plastic deformation of the particles, together with crack deflection

* Corresponding author. Tel.: +1-510-486-5798; fax: +1-510-486-4881.

E-mail address: roritchie@lbl.gov (R.O. Ritchie).

and interfacial debonding, provide the main contributions to toughness [2–7]. Since molybdenum silicides with Si concentrations less than those of MoSi_2 , i.e. Mo_5Si_3 and Mo_3Si , suffer from poor oxidation resistance, boron is added in the current alloy to promote oxidation resistance by forming protective borosilicate glass [8]. It has been reported that the addition of as little as 1 wt.% boron improved the oxidation resistance by as much as five orders of magnitude at moderate to high temperatures (800–1500°C) [1]. Consequently, the current alloy was processed with a composition of Mo–12Si–8.5B (at.-%), such that it contained the α -Mo, Mo_3Si , and Mo_5SiB_2 (T2) phases. Indeed, the toughness of this material was expected to be higher than that of MoSi_2 due to the presence of the relatively ductile Mo phase, which in this microstructure appears to form as isolated α -Mo particles in the $\text{Mo}_3\text{Si}/\text{Mo}_5\text{SiB}_2$ matrix (Fig. 1).

It is the objective of the present work to examine the fracture toughness (R-curve) and fatigue-crack growth characteristics of this Mo–12Si–8.5B alloy, both at ambient and elevated temperatures up to 1300°C, and to discern the salient mechanisms governing crack growth.

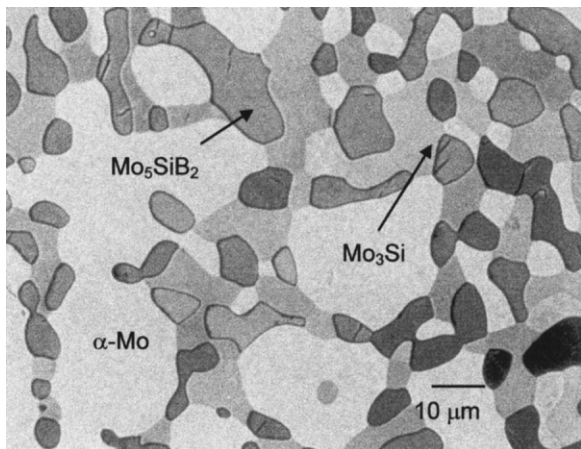


Fig. 1. Scanning electron micrograph of the Mo–12Si–8.5B (at.-%) alloy, showing α -Mo particles in the $\text{Mo}_3\text{Si}/\text{Mo}_5\text{SiB}_2$ matrix (etched with Murakami's reagent).

2. Materials and experimental procedures

The Mo–12Si–8.5B (at.-%) alloy was prepared by arc melting in a partial pressure of argon (70 kPa) and drop-casting into water-cooled copper molds with a diameter of 25 mm. The elemental Mo, Si, and B were 99.95, 99.99 and 99.5 wt.% pure, respectively. Ingots were homogenized in vacuo for 24 h at 1600°C. Further details on the processing and microstructural characterization of this material are reported elsewhere [9,10]. Mechanical property measurements for this alloy at ambient temperature gave a three-point bend strength of ~500 MPa [10]. Additionally, other room-temperature physical and mechanical properties of the constituents, α -Mo, Mo_3Si , and Mo_5SiB_2 (T2) phases are presented in Table 1. The hardness properties listed in the table were evaluated using a Vickers indentor at 100 g load using a Buehler Micromet microhardness tester. Among the brittle materials comprising the matrix, Mo_5SiB_2 phase assumes higher hardness values (~18–19 GPa) than Mo_3Si phase (~15 GPa) which is roughly consistent with the reported values for the Mo_3Si phase of 13–13.5 GPa [13,14].

Cyclic fatigue-crack growth rate measurements were performed at ambient temperature in a controlled room-air environment and at elevated temperatures (800–1300°C) in flowing gaseous argon. Testing was performed with disk-shaped compact-tension DC(T) specimens (of width 17.8 mm, and thickness 2.8 mm), containing "large" (>3 mm) through-thickness cracks. Specimens were cycled under load and/or stress-intensity control on a computer-controlled, servo-hydraulic mechanical test frame with a test frequency of 25 Hz (sinusoidal waveform) and at a constant load ratio ($R = K_{\min}/K_{\max}$) of 0.1 (where K_{\max} and K_{\min} are, respectively, the maximum and minimum stress intensities in the fatigue cycle). Crack-growth rates, da/dN , were determined over the range $\sim 10^{-11}$ – 10^{-5} m/cycle under computer-controlled K -decreasing and K -increasing conditions. Data are presented in terms of the applied stress-intensity range ($\Delta K = K_{\max} - K_{\min}$). Fatigue thresholds, ΔK_{TH} , below which large cracks are

Table 1
Physical and mechanical properties of the individual phases in the Mo–12Si–8.5B alloy^a

Property	Mo	Mo_3Si	Mo_5SiB_2
Melting point (°C)	2610	2025	2160–2200
Crystal structure	BCC	Cubic A15	Tetragonal D8 _I
Elastic modulus, E (GPa)	324	295	—
Density (g/cm ³)	10.22	8.9	8.8
Microhardness (GPa)	7.1	15	18.5
Coefficient of thermal expansion, α at 25° (K) at 1300°C (K)	$\sim 5 \times 10^{-6}$ $\sim 6 \times 10^{-6}$	$\sim 3 \times 10^{-6}$ $\sim 7 \times 10^{-6}$	$\sim 6 \times 10^{-6}$ $\sim 8.5 \times 10^{-6}$
Volume fraction (%)	38.4	31.8	29.8

^a Compiled from Refs. [11–15].

presumed to grow at vanishingly small rates, were operationally defined as the maximum value of ΔK at which growth rates did not exceed 10^{-10} m/cycle.

Prior to data collection, samples were fatigue pre-cracked for a few millimeters beyond the notch. Owing to the brittleness of the material, the initiation of the precrack was one of the most critical procedures in the test. In the current work, crack initiation was facilitated using a half-chevron shaped notch, sharpened by razor micro-notching (Fig. 2). The latter process involves running an extra keen single edge blade, with a thickness of 230 μm , at roughly constant pressure across the bottom of the notch in the presence of 1- μm diamond polishing fluid. After razor micro-notching, the crack tip radius was on the order of 5–10 μm , i.e. approximately an order of magnitude smaller than the machined notch.

For room temperature testing, crack lengths were continuously monitored using unloading elastic-compliance measurements with a 350- Ω strain gauge attached to the back-face of the specimen [16]. At elevated temperatures, an electrical potential-drop technique was used to similarly monitor crack lengths [17,18]. The use of this technique was feasible in the present case as the electrical conductivity of Mo–12Si–8.5B alloy is quite high (the resistivity is $< 1 \Omega \text{ cm}$) compared to common ceramic materials. In the present tests, a constant direct current of $\sim 2 \text{ A}$ was applied to the sample, such that an initial (amplified) output potential of between ~ 0.4 and 0.6 V was developed across the starter crack. Subsequent changes in the output potential were normalized by this initial voltage, and then continuously measured to permit in situ monitoring of crack length. Complete details on this technique are given in Refs. [18].

The fracture toughness was evaluated using resistance curve (R-curve) methods, which were determined by loading pre-cracked DC(T) specimens to failure under monotonically increasing loads under displacement

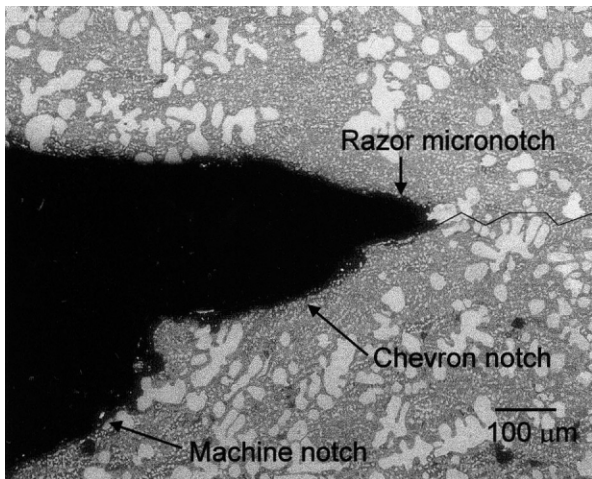


Fig. 2. Scanning electron micrograph of a pre-cracked Mo–12Si–8.5B alloy showing notches of different sizes created for tests, i.e. machine notch, chevron notch, and razor micronotch, respectively.

control. During such tests, crack lengths were periodically monitored using the same procedures (unloading back-face strain compliance at room temperature, electrical potential methods at high temperatures); unloading excursions were limited to less than 10% of the current load. Following pre-cracking, specimens were cycled for $\sim 24 \text{ h}$ at the ΔK_{TH} threshold, where no discernable crack growth occurs; this procedure was intended to minimize the effect of any pre-existing crack-tip shielding (primarily crack bridging) on the subsequently measured initiation toughness, K_o . Indeed, comparison of R-curve from a fatigue-precracked sample with that of a razor-micronotched sample, where the presence of near-tip crack-wake bridging would be nonexistent, suggests that the effect of bridging grains in the wake of the fatigue pre-crack was minimal (Fig. 3). It should be noted here that since the latter tests all involve nominally atomically-sharp cracks, measured toughness values may be smaller than values obtained from other methods that rely on a machined notch as the initial crack [10]. Data are presented in terms of crack-growth resistance, K_R , plotted as a function of the crack extension, Δa .

Due to the difficulty of determining the extent of R-curve toughening over the initial hundred micrometers of crack growth with macroscopic testing techniques, a so-called micro R-curve was also determined using an in situ scanning electron microscope (SEM) stage (see Ref. [19]). Identical, fatigue-precracked DC(T) specimens were loaded in displacement control in increments of $\sim 2\text{--}3 \text{ N}$ until crack growth was detected, whereupon the crack length was measured by imaging the crack in the SEM to an accuracy of $\sim 1 \mu\text{m}$.

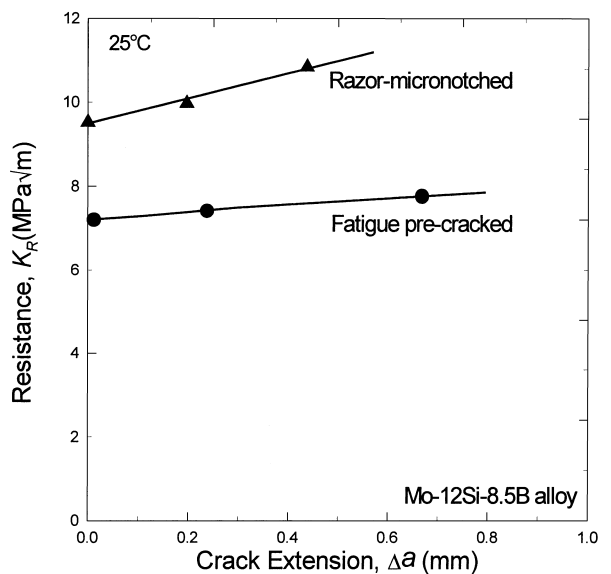


Fig. 3. The resistance curve behavior of a razor-micronotched specimen, compared with that of a fatigue pre-cracked specimen, exhibiting no significant grain bridging effect in the wake of the precrack.

Fatigue and fracture morphologies were examined in a scanning electron microscope and from crack-path profiles, obtained by metallographic sectioning at the specimen mid-thickness perpendicular to the crack plane. Measurements of the size and proportion of cracked and decohered α -Mo particles involved in crack advance were carried out using a direct-counting technique on both fracture surfaces and crack path profiles.

3. Results

3.1. Resistance-curve behavior

Measurements of the fracture toughness and R-curve behavior using conventional unloading elastic-compliance techniques indicate relatively large crack-initiation toughnesses in Mo–12Si–8.5B (Fig. 4). Compared to a K_c value of $\sim 3\text{--}4 \text{ MPa}\sqrt{\text{m}}$ in monolithic MoSi₂ [4], the initiation toughness in Mo–12Si–8.5B at room temperature is $\sim 7.2 \text{ MPa}\sqrt{\text{m}}$, i.e. over 70% higher. However, most of the toughening appears to be intrinsic, i.e. not involving crack-tip shielding, as the subsequent R-curve is very shallow. Mechanistically, metallographic observations show only minimal interaction between the α -Mo particles and the crack path at ambient temperatures (Fig. 5a); indeed, somewhat surprisingly, the Mo particles do not appear to provide any appreciable impedance to crack advance. The crack path is primarily confined to the matrix and the Mo/matrix interface. From direct-counting techniques, approximately 50%

of the Mo particles (which in total comprise 38 vol.% of the microstructure) cracked through the particles, the remainder failed along the interface. Specifically, the crack tended to circumvent the relatively small (less than $\sim 5 \mu\text{m}$) Mo particles with spherical shape and to propagate through them when they were relatively large with elongated shape. Of note is the fact that there is little evidence of plastic stretching as the Mo phase is traversed by the crack; this is consistent with the minimal crack-growth resistance associated with crack extension on the R-curve (Fig. 4).

Only minimal rising R-curve behavior with a relatively high initiation toughness was detected, based on data obtained from a back-face unloading compliance technique to monitor crack extension. This suggests that the toughening effect for the Mo–12Si–8.5B alloy at room temperature results from mechanisms other than crack bridging, i.e., crack trapping and the subsequent crack renucleation across the ductile particle. However,

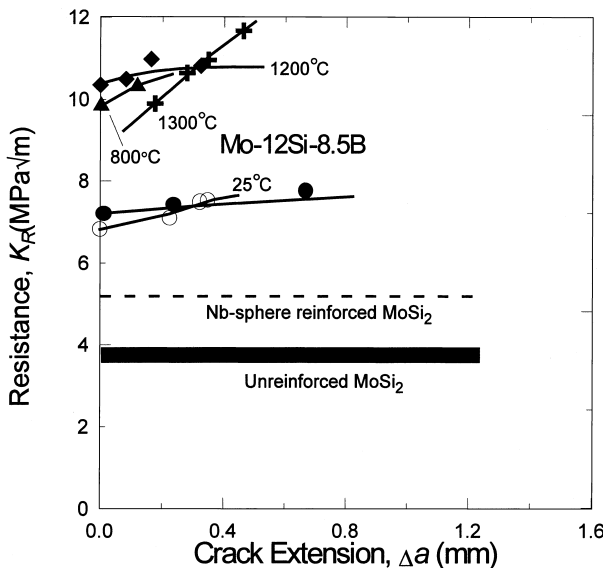


Fig. 4. Fracture toughness behavior, in the form of K_R (Δa) crack-growth resistance curves, for Mo–12Si–8.5B alloy both at ambient and elevated temperatures, as compared to published results [4,20] on MoSi₂ reinforced with Nb spheres. For the 25°C data, symbol ● represents data points from macroscopic compliance measurements and symbol ○ represents in situ study results.

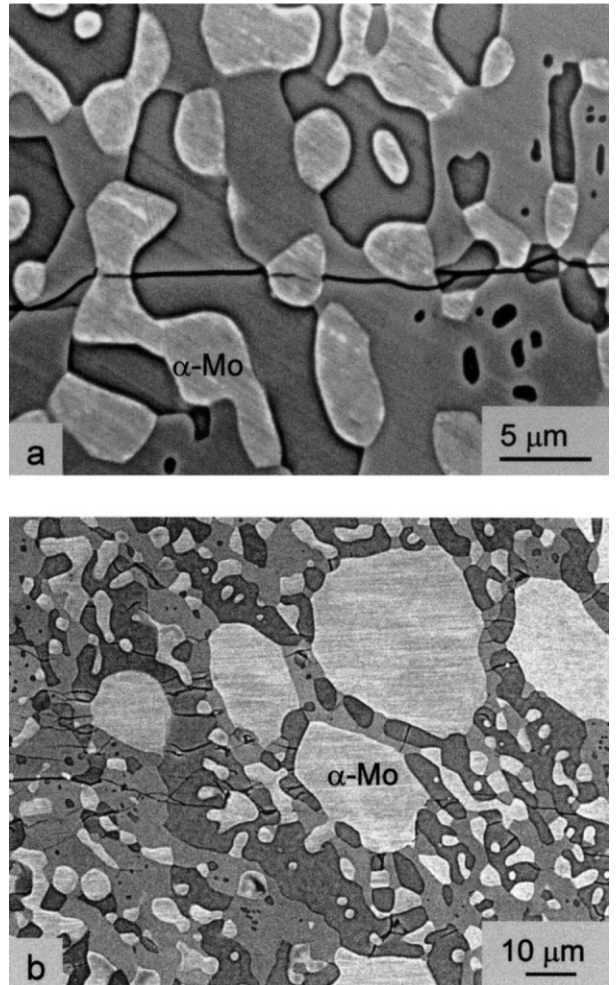


Fig. 5. Scanning electron micrographs of crack paths under monotonic loading in the Mo–12Si–8.5B alloy, showing the interaction of the crack with the microstructure, at (a) ambient (25°C) and (b) elevated (1300°C) temperatures. The direction of crack growth is from left to right.

an alternative explanation can be that the dimensions over which crack bridging is occurring are too small to be detected by conventional unloading compliance techniques. Accordingly, the micro R-curve behavior was determined using an *in situ* tensile loading stage in the SEM. Results from the *in situ* testing at ambient temperature are shown in Fig. 4 and indicate minimal differences between the R-curves measured *in situ* and by conventional compliance techniques. Specifically, the Mo–12Si–8.5B exhibits a quite flat R-curve behavior with toughness increasing from $K_0 \sim 6.85 \text{ MPa}\sqrt{\text{m}}$ ($\sim 7.2 \text{ MPa}\sqrt{\text{m}}$ with unloading compliance) to a maximum value of $K_c \sim 7.52 \text{ MPa}\sqrt{\text{m}}$ ($\sim 7.75 \text{ MPa}\sqrt{\text{m}}$ with unloading compliance). We thus conclude that the toughening in Mo–12Si–8.5B at room temperature does not primarily originate from shielding, e.g. crack bridging, in the wake of the crack tip; rather, it appears to be associated with intrinsic mechanisms active ahead of the tip, specifically in the form of crack trapping. Fig. 6a–d shows a sequence of crack advance during the *in situ* R-curve measurements. Fig. 6a depicts the initial fatigue pre-crack trapped at a large ductile α -Mo particle at zero load at the beginning of the test. With increasing stress intensity ($K \sim 6.5 \text{ MPa}\sqrt{\text{m}}$), several microcracks form

around the main crack tip and open up (Fig. 6b and c). No difference in crack length was observed until stress intensity at the crack tip, $K \sim 6.9 \text{ MPa}\sqrt{\text{m}}$, where the crack begins to propagate through the α -Mo particle (Fig. 6d) and extends $\sim 200 \mu\text{m}$ before arresting at the next α -Mo particle.

At elevated temperatures, the intrinsic toughness of the Mo–12Si–8.5B alloy is significantly increased, to over $10 \text{ MPa}\sqrt{\text{m}}$ at 1200°C , again with very shallow R-curves, although at 1300°C , the R-curve does become somewhat steeper. As shown in Fig. 4, the crack-growth resistance at 1300°C steadily increased over the first $\sim 400 \mu\text{m}$ of crack extension, from an initial value of $K_0 \sim 9 \text{ MPa}\sqrt{\text{m}}$ to a maximum value of $K_c \sim 11.8 \text{ MPa}\sqrt{\text{m}}$. The presence of some degree of crack-growth toughening at this temperature is consistent with metallographic observations (Fig. 5b) which do show evidence of crack bridging by unbroken α -Mo particles in the crack wake. However, as discussed below, also apparent is that the ductile-particle bridging additionally occurs within an extensive network of microcracking parallel to the main crack; indeed, the microcracks all appear to be arrested at the α -Mo regions, presumably because of the increased ductility of the Mo at this temperature.

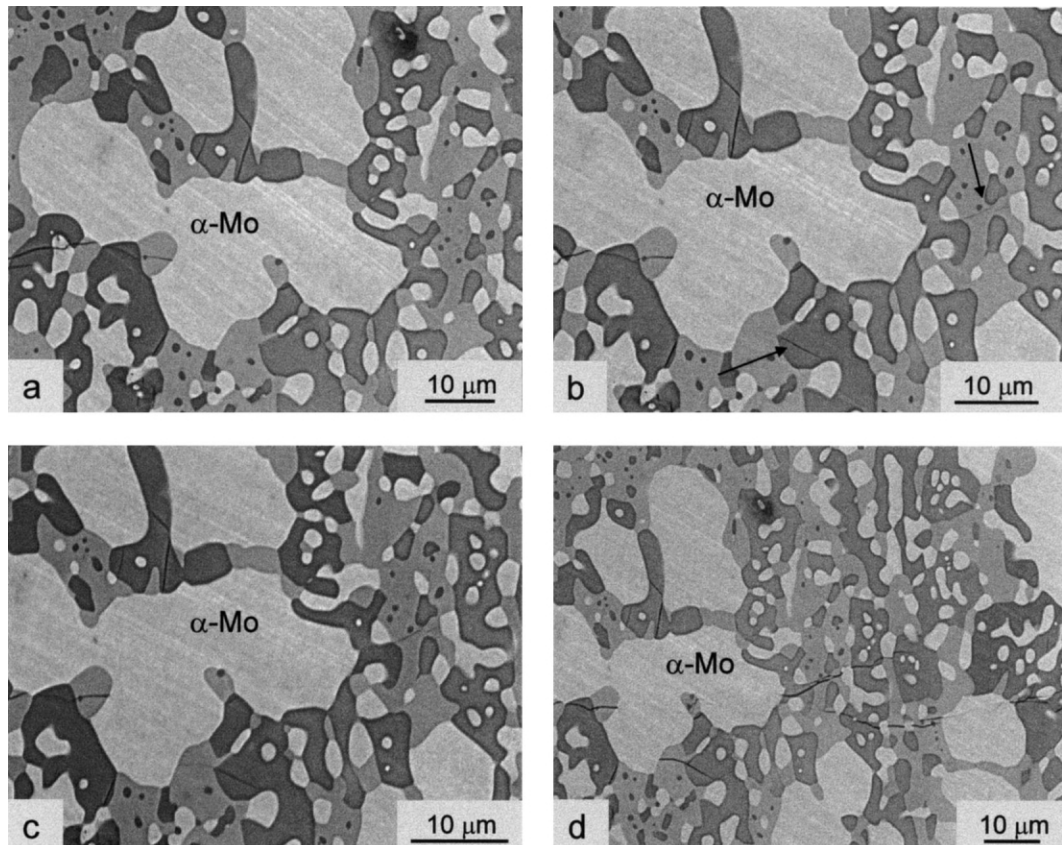


Fig. 6. *In situ* scanning electron micrographs illustrating the development of microcracking ahead of the crack tip during the extension of the main crack. Figures show (a) the initial fatigue pre-crack, (b) microcrack formation in the matrix ahead of the crack tip, (c) opening up of the main crack and surrounding microcracks, and (d) propagation of the main crack through α -Mo particles. The direction of crack growth is from left to right.

3.2. Fatigue-crack growth behavior

The variation in fatigue-crack propagation rates with the applied stress-intensity range for the Mo–12Si–8.5B alloy is shown in Fig. 7; results are plotted for ambient and elevated (800, 1200, and 1300°C) temperatures and are compared with previous results on monolithic and composite MoSi₂ [4,20]. It is apparent that the fatigue-crack growth properties of this alloy are superior to that of monolithic MoSi₂; indeed, at 25°C, the ΔK_{TH} threshold in Mo–12Si–8.5B of ~ 5 MPa \sqrt{m} is significantly larger than the fracture toughness of MoSi₂. Moreover, threshold values are even higher at elevated temperatures, rising to over 7 MPa \sqrt{m} above 1200°C. Indeed, like the fracture toughness values, the fatigue threshold values are progressively enhanced with increasing temperature. Also of note is that it has been claimed that there are no ‘pest’ reactions in B-doped Mo silicides at 800°C [1], in contrast to monolithic MoSi₂ which can exhibit ‘pest’ oxidation at intermediate temperatures [1,4].

Characteristic of brittle materials at low homologous temperatures [21], crack-growth rates in Mo–12Si–8.5B exhibit a marked sensitivity to the stress intensity. In terms of the Paris power-law relationship, $da/dN = C\Delta K^m$ (where C and m are scaling constants), the Paris exponents are $m \sim 60$ at 25°C and ~ 55 both at 800 and 1200°C. This implies that this material is essentially not susceptible to premature failure by fatigue, particularly at the lower temperatures. There are good mechanistic reasons for this. Cyclic fatigue in brittle materials, e.g. ceramics and intermetallics, results from a conceptually different

mechanism to that of the well known metal fatigue; specifically it arises from a progressive (cycle-dependent) degradation in extrinsic (R-curve) toughening behind the crack tip [21]. Except for a limited extent at 1300°C, the Mo–12Si–8.5B alloy is toughened primarily by intrinsic mechanisms, as is apparent by the comparatively high initiation toughnesses and relatively flat R-curves (Fig. 4). Thus, since there is only limited extrinsic toughening to degrade, this alloy shows only minimal susceptibility to fatigue failure. The cyclic fatigue resistance of the Mo–12Si–8.5B alloy is further improved with increase in temperature up to 1300°C. Specifically, the ΔK_{TH} fatigue threshold was increased, by $\sim 50\%$ compared to room temperature, to ~ 7.5 MPa \sqrt{m} . However, the development of some degree of extrinsic toughening at the temperature, due to crack bridging by the α -Mo phase, does lead to a marginally increased susceptibility to fatigue, i.e. the Paris exponent is reduced somewhat to $m \sim 44$. No appreciable evidence of creep damage mechanisms, e.g., in the form of cavitation damage, could be found at 1300°C.

4. Discussion

4.1. General considerations

The toughening of brittle solids through the inclusion of ductile phase is generally accomplished extrinsically, i.e. through the development of crack-tip shielding from crack deflection and/or crack bridging by intact ductile particles in the crack wake [e.g. 21–23]; such mechanisms invariably lead to rising R-curve behavior (crack-growth toughening) but can result in susceptibility to fatigue failure as they have a tendency to degrade under cyclic loading [21]. In the case of ceramics or intermetallics for high-temperature applications, the choice of reinforcements is limited to the refractory metals such as Mo, Nb, Cr and W due to their high melting temperature, although many of these refractory metal reinforcements do not exhibit significant ductility at room temperature [15]. Consequently, if the crack can be arrested at the ductile phase such that it must renucleate on the other side, the resultant crack trapping acts to toughen the material intrinsically, as schematically shown in Fig. 8a and b. It is apparent that significant crack trapping by the α -Mo phase occurs in the Mo–12Si–8.5B alloy, particularly at lower temperatures. The importance of this is that the toughening mechanism is intrinsic and thus will not necessarily degrade under cyclic loads [21,24]. However, if the ductility of the trapping phase is sufficiently high to remain intact in the wake of the crack tip, it can additionally act extrinsically as crack bridges. Shielding by crack bridging, shown schematically in Fig. 8c, is known to be an effective toughening process in many monolithic and

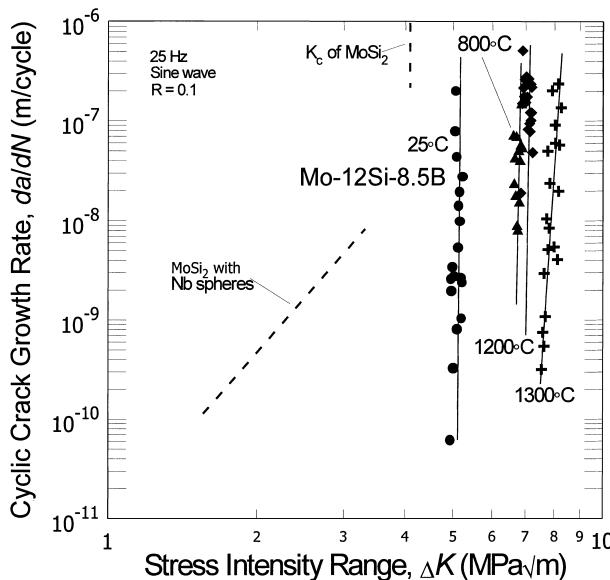


Fig. 7. Cyclic fatigue-crack propagation data of Mo–12Si–8.5B alloy as a function of applied ΔK at 25, 800, 1200, and 1300°C, compared to published results [4,20] on monolithic MoSi₂ and MoSi₂ reinforced with Nb spheres.

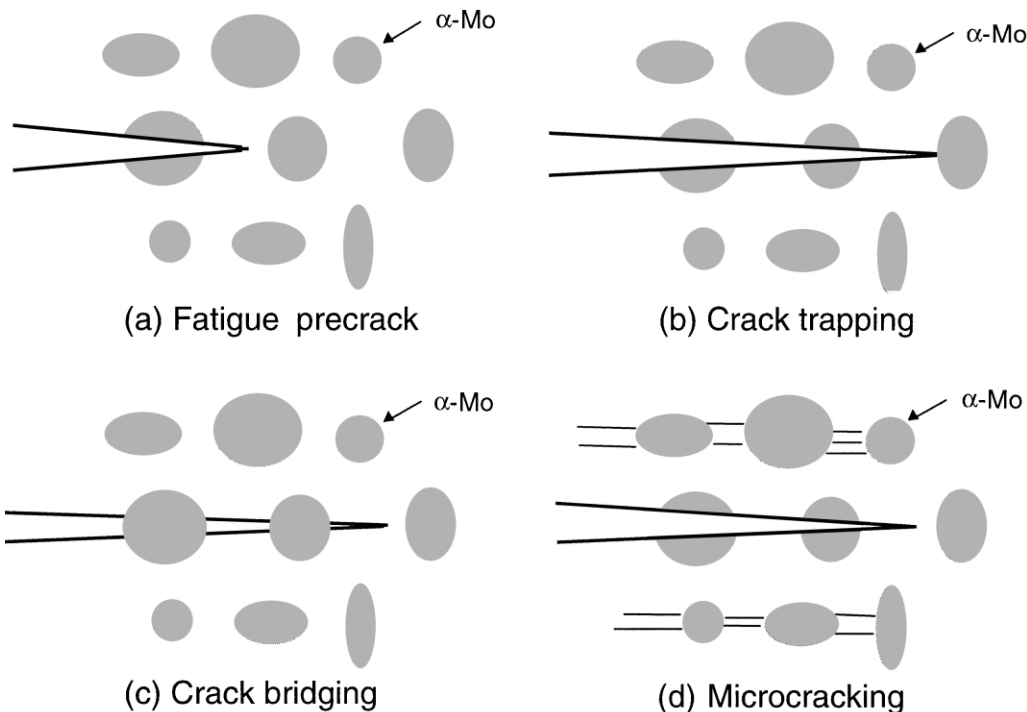


Fig. 8. Schematic illustrating dominant toughening mechanisms in the Mo–12Si–8.5B alloy: (a) fatigue precrack; (b) crack trapping; (c) crack bridging; and (d) microcracking.

composite intermetallics and ceramics [24–28]. As discussed below, it is not an active mechanism in Mo–12Si–8.5B at ambient temperatures owing to the low ductility of the Mo phase; however, at elevated temperatures, it is clearly far more potent. Finally, the Mo–12Si–8.5B alloy shows extensive stress-induced microcracking at elevated temperatures. This process, shown schematically in Fig. 8d, can occur in brittle materials, such as ceramics and rocks, in the vicinity of the crack tip, specifically within regions of local residual tension caused by thermal expansion mismatch and/or by transformation [29,30]; in simple terms, its effect is largely to induce a dilatation in the microcracking zone surrounding the crack wake.

4.2. Toughening mechanisms at ambient temperatures

In the current Mo–12Si–8.5B alloy, Fig. 6a–d shows the interaction of the α -Mo phase with the main crack during crack extension at ambient temperature under monotonic loading. Microcracks can be seen to form around the crack tip as the main crack is arrested at a Mo particle; further microcrack formation then occurs as the crack renucleates on the far side of the particle. Such crack trapping accompanied by microcracking appears to provide the main source of (intrinsic) toughening at lower temperatures. As the vast majority of the α -Mo particles intersected by the crack do not remain intact in the crack wake (Fig. 5a), presumably because

of the limited ductility of Mo at 25°C¹, there is insignificant crack bridging and hence little crack-growth toughening. Accordingly, the R-curve is relatively shallow and susceptibility to fatigue is minimal. The failure of the Mo phase is shown in Fig. 9; fracture at room temperature is quite brittle (Fig. 9a), as reported in refs. [33,34], whereas at 1300°C, the Mo particles debond from the $\text{Mo}_3\text{Si}/\text{Mo}_5\text{SiB}_2$ matrix with significant amounts of plastic stretching (Fig. 9b). As discussed below, such increased ductility of the Mo particles does result in some degree of wake bridging in the Mo–12Si–8.5B alloy at elevated temperatures.

Thus, based on in situ observations of the crack/ α -Mo interactions (Fig. 6), crack trapping appears to be the dominant toughening mechanism in Mo–12Si–8.5B at ambient temperatures. The process involves crack arrest at an α -Mo particle, subsequent microcrack formation ahead of the crack tip and, with increasing stress intensity, renucleation across the particle achieved by the remainder of the crack either bowing out between the pinning regions or propagating through the particle. The extent of toughening can be estimated in terms of the relative toughness of the “composite”, K_c^c , and matrix, K_c^m [35]:

¹ Depending on purity, the ductile–brittle transition temperature of molybdenum is of the order of ~50–500°C [31,32].

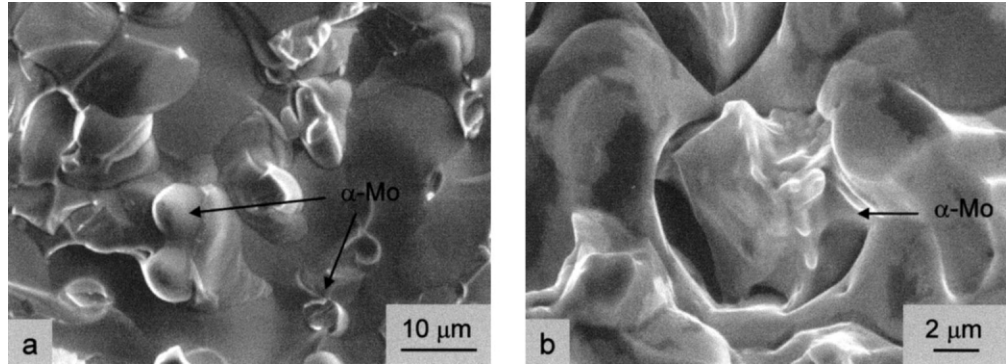


Fig. 9. Scanning electron micrographs of the fracture surfaces in the Mo-12Si-8.5B alloy, showing (a) no evidence of plastic deformation of Mo phase at ambient temperature, and (b) significant amount of plastic stretching and debonding of the Mo phase from the brittle $\text{Mo}_3\text{Si}/\text{Mo}_5\text{SiB}_2$ matrix at 1300°C.

$$\frac{K_c^c}{K_c^m} = \left\{ 1 + \frac{2r}{l} \left[\left(\frac{K_c^p}{K_c^m} \right)^2 - 1 \right] \right\}^{1/2} \quad (1)$$

where r is the characteristic dimension of the trapping phase, l is the average spacing (not necessarily the particle spacing, but the distance between the particles where the crack is trapped), and K_c^p is their toughness. Using a fracture toughness for Mo at 25°C of 15 MPa $\sqrt{\text{m}}$ [22,36] and for the matrix of 3.5 MPa $\sqrt{\text{m}}$ [10], and an average value r/l of ~ 0.2 (based on crack profile measurements), Eq. (1) predicts a toughness due to crack trapping of 9.8 MPa $\sqrt{\text{m}}$, which, considering the uncertainties in the toughness values², is reasonably close to the experimentally measured values.

4.3. Toughening mechanisms at elevated temperatures

4.3.1. Ductile-phase toughening

As noted above, the increased ductility of the α -Mo phase at elevated temperatures promotes some degree of ductile-phase bridging (Fig. 5b), which at 1300°C results in a rising R-curve. Quantitatively, the magnitude of such toughening can be estimated from the increase in energy associated with particle deformation and failure in the wake of the crack [26]. Assuming that small-scale bridging conditions apply, i.e. the bridging zone is small compared to crack length and specimen dimensions, the steady-state toughness can be determined from the dimensionless work of rupture of the reinforcement, or the area under the normalized stress [$\sigma(u)$]-displacement [u] function, as $\chi = \int_0^{u^*} (\sigma(u)du/\sigma_0 r)$, where σ_0 is the yield strength of the ductile phase, and u^* is the critical crack-opening displacement for its fracture [26,27]. The corresponding steady-state toughness, K_{ssb} , is then given by:

$$K_{\text{ssb}} = \sqrt{K_t^2 + fE' \sigma_0 r \chi} \quad (2)$$

where K_t is the crack initiation toughness of the “composite” (approximately the matrix toughness), E' is the plane-strain elastic modulus of the “composite”, and f is the volume fraction of bridging phase. Taking values at 1300°C for E' for Mo-12Si-8.5B of ~ 179 GPa and σ_0 for α -Mo of ~ 103 MPa [9,10,20], with a volume fraction of α -Mo of $f \sim 0.38$ with $r \sim 5 \mu\text{m}$, Eq. (2) predicts a value of K_{ssb} of ~ 10.8 MPa $\sqrt{\text{m}}$, assuming a matrix toughness of $K_t \sim 3.5$ MPa $\sqrt{\text{m}}$ [10] and an estimated value of χ of 3, based on the tensile properties of Mo at 1300°C [23,37]. Although only a rough estimate, the predicted toughness is comparable to the experimentally measured value of 11.7 MPa $\sqrt{\text{m}}$ at 1300°C.

4.3.2. Microcracking toughening

The other potential source of toughening in the Mo-12Si-8.5B alloy at elevated temperatures arises from microcracking. This can be seen in Fig. 5b as a zone of microcracks, arrested between α -Mo particles, in layers parallel to the main crack. Most of the microcracks are formed in the Mo_5SiB_2 phase (Fig. 10), presumably because of the anisotropy in its thermal expansion resulting from its tetragonal crystal structure (both Mo and Mo_3Si are cubic).

The formation of such a zone of microcracks around the crack tip can be considered as analogous to the crack-tip plastic zone in metals, which dissipates energy through work done in the opening and sliding displacements involved in microcracking and through creation of new surfaces [38–45]. In addition, the microcracks increase the compliance of the solid and can act as a mechanism of extrinsic toughening by shielding the crack tip from the remote stresses [39]. Controlled micro-cracks can be formed most effectively by a dispersion of a second phase, where tensile stresses develop around this phase when its thermal expansion coefficient is lower than that of the matrix [40,41]. As the coefficient of thermal

² Small amounts of interstitial impurities, such as oxygen, are known to severely embrittle Mo to below 5% elongation at ambient temperatures [36].

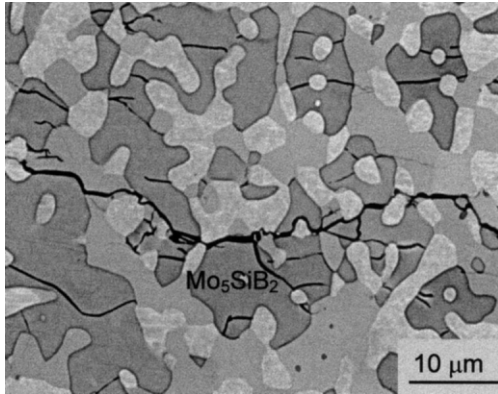


Fig. 10. Development of parallel microcracks around the crack tip in the Mo–12Si–8.5B alloy during cyclic fatigue-crack propagation at 1300°C. The crack growth is from left to right.

expansion of Mo at 1300°C ($6 \times 10^{-6} \text{ K}^{-1}$ [31]) is lower than that of Mo_5SiB_2 ($8.5 \times 10^{-6} \text{ K}^{-1}$ [46]), it would be expected that the microcracking should form in the latter phase, and be parallel to the main crack, i.e. perpendicular to the applied tensile stresses. This orientation of microcracking is particularly effective in promoting toughening, as microcracks located parallel to the main crack can more easily extend and coalesce within the process zone, and hence are more effective in absorbing energy before the major crack can propagate [40].

Although microcrack toughening has only been rigorously identified for a limited number of materials, including Al_2O_3 toughened with ZrO_2 , SiC toughened with TiB_2 , and Ti–6Al–4V reinforced with TiC , the effect is known to involve the dilatation associated with the volume displaced by the microcracks and the reduction in the elastic modulus within the process zone. During the microcracking process, the volume change involved in the vicinity of the crack tip introduces a nonlinear stress-strain response as shown in Fig. 11a [29,39]; on unloading, this results in closure forces on the crack wake [47], similar to transformation toughening [48]. An estimation of the closure stress intensity at steady-state for such dilatational toughening gives [43,47]:

$$\Delta K_d \approx 0.22\epsilon E' f_m \sqrt{h} \quad (3)$$

where $E' = E$, Young's modulus, in plane stress, and $E/(1-v^2)$ in plane strain (v is Poisson's ratio), f_m is the volume fraction of microcracks, ϵ is the dilatational strain, and h is the height of microcrack zone (Fig. 11b). E for this alloy has been reported to be 327 GPa [9]. In addition, direct measurements of crack profiles obtained at 1300°C gave the approximate values of the volume fraction of microcracks in the microcracking zone as $f_m \sim 0.15$, the height of this zone to be $h \sim 20 \mu\text{m}$, and the residual volumetric strain, ~ 0.06 . This yields an estimate of the maximum dilatational toughening of $\Delta K_d \sim 3 \text{ MPa}\sqrt{\text{m}}$.

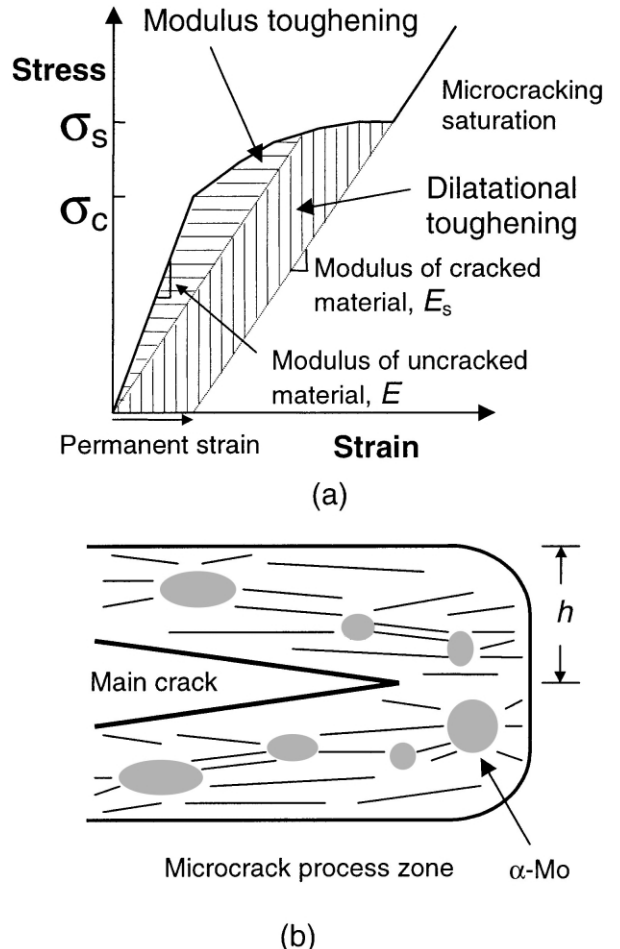


Fig. 11. (a) nonlinear stress–strain curve behavior as a result of microcracking [29,39] and (b) microcracking process zone.

The reduction in modulus associated with the presence of the microcracks also contributes to the toughening [39,49]:

$$\Delta K_m \approx \beta f_m K_t \quad (4)$$

where $\beta \sim 1.2$ [49] is a parameter depending on Poisson's ratio and the (untoughened) matrix toughness, $K_t \sim 3.5 \text{ MPa}\sqrt{\text{m}}$ [10]; for the Mo–12Si–8.5B alloy, Eq. (4) yields a value of ΔK_m of $\sim 1 \text{ MPa}\sqrt{\text{m}}$. These estimates suggest a total increase in toughness on the order of 4 MPam due to microcracking, which is roughly consistent with experimental observations (Fig. 4).

In summary, it has been shown that the boron-modified molybdenum silicide alloy, Mo–12Si–8.5B, can be processed to be considerably tougher and more fatigue resistant than monolithic MoSi_2 . Moreover, its crack-growth resistance, in both fracture and fatigue, progressively increases with increase in temperature up to 1300°C. This is due to the onset of additional toughening mechanisms at elevated temperatures, specifically, ductile-phase toughening by $\alpha\text{-Mo}$ and microcracking in

Mo_5SiB_2 , which arrest at the α -Mo phase. Despite such toughening, which clearly is in large part associated with the presence of the primary Mo phase, it is this same microstructural constituent that results in a lower oxidation resistance compared to MoSi_2 . Clearly, if molybdenum silicides are ever to be seriously contemplated as ultrahigh temperature structural materials, alloys displaying both low-temperature toughness and high temperature strength/oxidation resistance will still need to be developed.

5. Conclusions

The ambient to elevated temperature fracture and fatigue-crack propagation behavior of a boron-modified, molybdenum silicide based alloy, Mo–12Si–8.5B (at.%), has been examined at 25–1300°C with the aim of discerning the salient mechanisms responsible for crack-growth resistance. Based on this work, the following conclusions can be made:

1. Compared to a fracture toughness of 3–4 MPa $\sqrt{\text{m}}$ in monolithic MoSi_2 , Mo–12Si–8.5B displays a K_c of ~ 7 MPa $\sqrt{\text{m}}$ at ambient temperatures, which rises to over 10 MPa $\sqrt{\text{m}}$ at 1200°C. Over this temperature range, however, the associated R-curves are relatively flat, inferring that such toughening is primarily intrinsic in nature, i.e. affecting the crack-initiation toughness. Mechanistic studies indicate that microcracking and extensive crack trapping by the primary α -Mo phase are the principal mechanisms of toughening; however, due to the limited ductility of the Mo at these temperatures, the Mo phase rarely remains unbroken in the crack wake such that crack-tip shielding by ductile-phase bridging is minimal.
2. At 1300°C, conversely, some degree of ductile-phase bridging is evident, due to the presence of uncracked α -Mo regions in the crack wake; in addition, extensive microcracking (primarily in the Mo_5SiB_2 phase) can be seen in the form of a network of arrested cracks parallel to the main crack. Since both the mechanisms are extrinsic in nature, i.e. affecting the crack-growth toughness, the alloy displays rising R-curve behavior at this temperature, with a maximum toughness of 11.8 MPa $\sqrt{\text{m}}$.
3. The fatigue-crack growth resistance of the Mo–12Si–8.5B alloy at ambient temperatures is also superior to that of monolithic MoSi_2 ; indeed, its ΔK_{TH} fatigue threshold value of ~ 5 MPa $\sqrt{\text{m}}$ is significantly larger than the fracture toughness of MoSi_2 . ΔK_{TH} thresholds are further enhanced at elevated temperatures, rising to 7–7.5 MPa $\sqrt{\text{m}}$ at 1200°–1300°C. Due to the minimal role of extrinsic toughening (except at 1300°C), Paris power-law

exponents are extremely high, i.e. $m \sim 44$ to 60, such that the Mo–12Si–8.5B alloy can be considered to be only marginally susceptible to premature failure by fatigue at temperatures up to 1200°C.

4. In general, the Mo–12Si–8.5B alloy displays the desirable property of enhanced toughness and resistance to fatigue-crack growth with increase in temperature from ambient to as high as 1300°C. This is associated with the onset of additional toughening mechanisms at elevated temperatures, namely ductile-phase toughening by the α -Mo phase and microcracking in the Mo_5SiB_2 phase.

Acknowledgements

This work was supported by the Director, Office of Science, Office of Basic Energy Sciences, Materials Sciences Division of the US Department of Energy under Contract No. DE-AC03-76SF00098 and DE-AC05-00OR22725, as part of the multi-National Laboratory program on “Design and Synthesis of Ultrahigh-Temperature Intermetallics” within the DOE Center for Excellence for the Synthesis and Processing of Advanced Materials.

References

- [1] Akinc M, Meyer MK, Kramer MJ, Thom AJ, Huebsch JJ, Cook B. *Mater Sci Eng* 1999;A261:16–23.
- [2] Krstic VD, Nicholson PS, Hoagland RGJ. *Am Ceram Soc* 1981;64:499–504.
- [3] Ashby MF, Blunt FJ, Bannister M. *Acta Metall* 1989;37:847–57.
- [4] Venkateswara Rao KT, Soboyejo WO, Ritchie RO. *Metall Trans A* 1992;23A:2249–57.
- [5] Lu TC, Evans AG, Hecht RJ, Mehrabian R. *Acta Metall Mater* 1991;39:1853–62.
- [6] Hing P, Groves GWJ. *Mater Sci* 1972;7:422–6.
- [7] Sigl LS, Exner HE. *Metall Trans A* 1987;18A:1299–308.
- [8] Nowotny H, Kimakopoulou E, Kudeilka H. *Mh Chem* 1957;88:180–92.
- [9] Schneibel JH, Liu CT, Easton DS, Carmichael CA. *Mater Sci Eng* 1999;A261:78–83.
- [10] Schneibel JH, Kramer MJ, Ünal Ö, Wright RNJ. *Intermetallics* 2001;9:25–31.
- [11] Hampel CA. ed. Rare metals handbook 2nd ed. London: Reinhold Publishing Corporation. Chapman & Hall, 1961.
- [12] Schneibel JH, Liu CT, Heatherly L, Kramer MJ. *Scripta Mater* 1998;38:1169–76.
- [13] Misra A, Petrovic JJ, Mitchell TE. *Scripta Mater* 1999;40:191–6.
- [14] Samsonov GV, Vinitskii IM. Handbook of refractory compounds. New York: IFI/Plenum Company, 1980.
- [15] Davidson DL, Chan KS, Anton DL. *Metall Mater Trans A* 1996;27A:3007–18.
- [16] Gilbert CJ, McNaney JM, Dauskardt RH, Ritchie RO. *ASTM J Test Eval* 1994;22:117–20.
- [17] Chen D, Gilbert CJ, Zhang XF, Ritchie RO. *Acta Mater* 2000;48:659–74.
- [18] Chen D, Gilbert CJ, Ritchie RO. *ASTM J Test Eval* 2000;28:236–41.

- [19] Bencher CD, Sakaida A, Venkateswara Rao KT, Ritchie RO. *Metall Mater Trans A* 1995;26A:2027–33.
- [20] Badrinarayanan K, McKelvey AL, Venkateswara Rao KT, Ritchie RO. *Metall Mater Trans A* 1996;27A:3781–92.
- [21] Ritchie RO. *Int J Fracture* 1999;100:55–83.
- [22] Heredia FE, He MY, Lucas GE, Evans AG, Dèvre HE, Konitzer D. *Acta Metall Mater* 1993;41:505–11.
- [23] Chan KS. *Metall Trans A* 1992;23A:183–99.
- [24] Bloyer DR, Venkateswara Rao KT, Ritchie RO. *Metall Mater Trans A* 1999;30A:633–42.
- [25] Swanson PL, Fairbanks CJ, Lawn BR, Mai Y-W, Hockey BJ. *J Am Ceram Soc* 1987;70:279–89.
- [26] Dèvre HE, Evans AG, Odette GR, Mehranbian R, Emiliani ML, Hecht RJ. *Acta Metall Mater* 1990;38:1491–502.
- [27] Odette GR, Chao BL, Scheckherd JW, Lucas GE. *Acta Metall Mater* 1992;40:2381–9.
- [28] Venkateswara Rao KT, Odette GR, Ritchie RO. *Acta Metall Mater* 1994;42:893–911.
- [29] Evans AG, Faber KT. *J Am Ceram Soc* 1984;67:255–60.
- [30] Kotoul M, Profant T. *Mech Mater* 2000;32:203–34.
- [31] Tietz TE, Wilson JW. Behavior and properties of refractory metals. Stanford: Stanford University Press, 1965.
- [32] Koval AY, Vasilev AD, Firstov SA. *Int J Refract Met Hard Metls* 1997;15:223–6.
- [33] Shaw BJ. *Scripta Metall* 1969;3:815–20.
- [34] Furuya K, Nagata N, Watanabe R, Yoshida H. *J Nucl Metls* 1982;103-104:937–42.
- [35] Bower AF, Ortiz M. *J Mech Phys Solids* 1991;39:815–58.
- [36] Ramasundaram P, Bowman R, Soboyejo W. *Mater Sci Eng* 1998;A248:132–46.
- [37] Hall RW, Sikora PF. NASA Memo. 3-9-59E, 1959.
- [38] Hoagland RG, Embury JDJ. *Am Ceram Soc* 1980;63:404–10.
- [39] Hutchinson JW. *Acta Metall* 1987;35:1605–19.
- [40] Claussen N, Steeb J. *J Am Ceram Soc* 1976;59:457–8.
- [41] Claussen NJ. *Am Ceram Soc* 1976;59:49–51.
- [42] McMeeking RM, Evans AG. *J Am Ceram Soc* 1982;65:242–6.
- [43] Evans AG, Fu Y. *Acta Metall* 1985;33:1525–31.
- [44] Evans AG. *J Am Ceram Soc* 1990;73:187–206.
- [45] Rubinstein AA. *Int J Fracture* 1985;27:113–9.
- [46] Rawn CJ, Schneibel JH, Hoffman CM, Hubbard CJ. *Intermetallics* 2001;9:209–16.
- [47] Liu G, Zhu D, Shang JK. *Metall Mater Trans A* 1995;26A:159–66.
- [48] Evans AG, Heuer AH. *J Am Ceram Soc* 1980;63:241–8.
- [49] Sigl LS. *Acta Mater* 1996;44:3599–609.